

X-ray QSO evolution from a very deep ROSAT survey

L R Jones^{1,2}, I M McHardy², M R Merrifield², K O Mason³, P J Smith³,
 R G Abraham⁴, G Branduardi-Raymont³, A M Newsam¹, G Dalton⁵,
 M Rowan-Robinson⁶, G Luppino⁷

¹ Code 660.2, NASA/Goddard Space Flight Center, Greenbelt, MD 20771, USA.

² Department of Physics, The University, Southampton SO17 1BJ, UK.

³ Mullard Space Science Laboratory, University College London, Holmbury St Mary, Dorking RH5 6NT, UK.

⁴ Institute of Astronomy, University of Cambridge, Madingley Rd, Cambridge CB3 0EZ, UK.

⁵ Department of Astrophysics, University of Oxford, Keble Road, Oxford OX1 3RH, UK.

⁶ Astrophysics Group, Blackett Laboratory, Imperial College, London SW7 2BZ, UK.

⁷ Institute for Astronomy, University of Hawaii, 2680 Woodlawn Drive, Honolulu, Hawaii 96822, USA.

11 October 2018

ABSTRACT

In the deepest optically identified X-ray survey yet performed, we have identified 32 X-ray selected QSOs to a flux limit of 2×10^{-15} erg cm⁻² s⁻¹ (0.5–2 keV). The survey, performed with the ROSAT PSPC, has 89% spectroscopic completeness. The QSO log(N)-log(S) relation is found to have a break to a flat slope at faint fluxes. The surface density of QSOs at the survey limit is 230 ± 40 per square degree, the largest so far of any QSO survey. We have used this survey to measure the QSO X-ray luminosity function at low luminosities ($L_X < 10^{44.5}$ erg s⁻¹) and high redshifts ($1 < z < 2.5$). The highest redshift QSO in the survey has $z=3.4$. Combined with the QSOs from the *Einstein* EMSS at bright fluxes, we find pure luminosity evolution of the form $L_X \propto (1+z)^{3.0(+0.2, -0.3)}$ is an adequate description of the evolution of the X-ray luminosity function at low redshifts. A redshift cutoff in the evolution is required at $z=1.4^{+0.4}_{-0.17}$ (for $q_0=0.5$). We discuss the form of this evolution, its dependence on the model assumed and the errors on the derived parameters. We show that most previous X-ray surveys, including the EMSS, are consistent with a power law luminosity evolution index of 3.0.

The contribution of QSOs to the 1–2 keV cosmic X-ray background is found to be between 31% and 51%.

Key words: galaxies: active - quasars: luminosity function - cosmology: observations - diffuse radiation - X-rays.

1 INTRODUCTION

The evolution of the Active Galactic Nuclei population can be studied up to redshifts corresponding to $\approx 90\%$ of the age of the Universe, giving information on the nature of the AGN themselves and on the nature of the Universe at early epochs. Optical surveys (e.g. Boyle *et al.* 1991) have shown that pure luminosity evolution, in which the luminosity function simply moves to higher luminosities at higher redshifts, is a good description of QSO evolution at redshifts $0.3 < z < 2$. However, in the surveys of Hewett *et al.* (1993) and Miller *et al.* (1993) there is in addition a change in the slope of the luminosity function with redshift, such that the most luminous QSOs show no evidence for any evolution.

Optically, QSOs are proportionally very rare objects

which have to be carefully selected from the overwhelming number of galaxies and stars, usually using colour and morphological criteria based on well calibrated photographic plates. This selection of stellar objects produces incompleteness at low redshift, because the host galaxy may be resolved, and at low AGN luminosities, when the host galaxy may also contaminate the AGN colours. In contrast, X-ray surveys of AGN are very direct, since AGN are the most numerous type of source in current X-ray surveys.

The *Einstein* EMSS survey contains 427 QSOs with a median redshift of 0.3 (Maccacaro *et al.* 1991; Della-Ceca *et al.* 1992). (We use the term QSOs to refer to all broad line objects, including Seyfert 1 AGN and QSOs). ROSAT pointed surveys reach to fainter fluxes and higher redshifts. The RIXOS survey of Page *et al.* (1996) has a limiting flux

arXiv:astro-ph/9610124v1 16 Oct 1996

of 3×10^{-14} erg cm $^{-2}$ s $^{-1}$ (0.5-2 keV) and the survey of Boyle *et al.* (1994) reaches 4×10^{-15} erg cm $^{-2}$ s $^{-1}$. The results presented here are based on the UK ROSAT deep field survey. This is currently the faintest optically identified X-ray survey, reaching a flux limit of 2×10^{-15} erg cm $^{-2}$ s $^{-1}$, and is thus sensitive to QSOs of low luminosity ($L_X \sim 10^{44}$ erg s $^{-1}$) at redshifts up to $z=2$. The general properties of all the X-ray source populations detected in this survey, including the numerous narrow emission line galaxies detected at faint fluxes, are described in M^cHardy *et al.* (1996). The log(N)-log(S) relation of all X-ray sources combined has been investigated by Branduardi-Raymont *et al.* (1994) and Barcons *et al.* (1995). Romero Colmenero *et al.* (1996) have investigated the ROSAT X-ray spectra of the sources in this survey and shown that the mean X-ray spectral index of the QSOs is 0.92 ± 0.02 .

In section 2 we describe the X-ray and optical observations. In the following sections we explain our analysis technique and describe the results. In section 5 we discuss these results. Section 6 lists the conclusions.

2 OBSERVATIONS

2.1 X-ray Observations

Full details of both the X-ray and optical observations are given in M^cHardy *et al.* 1996. Here we summarize the main points. The survey field was selected for its low Galactic absorption, and ROSAT Position Sensitive Proportional Counter (PSPC) observations made at two epochs, giving a total exposure of 111 ksec. The inner 15 arcmin radius area of the combined exposure was searched for point-like X-ray sources. We used our own source detection software, employing a maximum-likelihood fit to the point spread function (Cash 1979) at each pixel of size 5 arcsec, and set the detection threshold so that one false source would be detected in the survey area. The increase in size of the point spread function (PSF) with off-axis angle, from a full width at half maximum (FWHM) of 25 arcsec on axis to a FWHM of 58 arcsec at 15 arcmin off axis (at an energy of 1 keV; Hasinger *et al.* 1993b), limited the survey to a radius of 15 arcmin. The 0.5-2 keV band was used to detect sources, rather than the full 0.1-2.4 keV ROSAT PSPC band, in order to reduce the background level and minimize the size of the instrumental PSF. There are 105 X-ray sources above 1.6×10^{-15} erg cm $^{-2}$ s $^{-1}$ in the 30 arcmin diameter survey region. We set the flux limit for a complete sample higher, at 2×10^{-15} erg cm $^{-2}$ s $^{-1}$ (0.5-2 keV), corresponding to 3.8σ confidence. Simulations showed that at this flux limit a log(N)-log(S) relation of the form measured by Branduardi-Raymont *et al.* (1994) could be successfully recovered, and thus that source confusion was not a major problem.

The limiting X-ray flux is a function of off-axis angle because of the strong increase in size of the PSF even within our survey region of 15 arcmin radius and because of mirror vignetting. The limiting flux was calculated in annuli of size 0.5 arcmin, including the PSF at 1 keV given by Hasinger *et al.* (1993b), the mirror vignetting, the background level and the shape of our survey area (two outer regions of the 15 arcmin radius circular area were not covered in our spectroscopic follow-up). The area of the annuli were then summed

Table 1. Area surveyed as a function of flux.

| Flux $\times 10^{-15}$ erg cm $^{-2}$ s $^{-1}$ (0.5-2 keV) | Sky area deg 2 | Effective sky area after correction for incompleteness |
|---|----------------------|--|
| 2.0 | 0.062 | 0.055 |
| 2.1 | 0.084 | 0.075 |
| 2.2 | 0.104 | 0.094 |
| 2.3 | 0.119 | 0.106 |
| 2.4 | 0.133 | 0.118 |
| 2.5 | 0.145 | 0.129 |
| 2.6 | 0.157 | 0.140 |
| 2.7 | 0.159 | 0.140 |
| 3.6 | 0.159 | 0.147 |
| 4.2 | 0.159 | 0.154 |
| 4.3 | 0.159 | 0.159 |

to give the total area surveyed as a function of flux. At fluxes $> 2.7 \times 10^{-15}$ erg cm $^{-2}$ s $^{-1}$ (0.5-2 keV) the area surveyed was 0.16 sq deg. The area surveyed at fainter fluxes is given in the second column of Table 1.

2.2 Optical Observations

Optical CCD imaging in V,R & I bands has been obtained at the University of Hawaii 88inch telescope, 2.5m Nordic Optical Telescope, 3.6m Canada-France-Hawaii Telescope (CFHT) and Michigan-Dartmouth-MIT 2.4m telescope. The deepest images reach at least $R=24.5$ mag. We have also made deep VLA radio maps at 20cm and 6cm, reaching a flux limit of 0.5 mJy at 20 cm. The ROSAT positions were corrected for the small ROSAT PSPC systematic position error using three independent methods (bright star/ROSAT coincidences, VLA/ROSAT coincidences, and the first few bright AGN spectroscopic identifications) which all gave a consistent offset of size 13 arcsec. A correction for the small ROSAT roll angle error of 0.185 degrees (Briel *et al.* 1995) was also applied. The remaining random error was 10 arcsec at 95% confidence. Most (90%) of the X-ray sources were identified with objects brighter than $R=23$ mag and $\approx 30\%$ had two or more possible counterparts of $R \leq 22.5$ mag.

Low resolution spectroscopy (10-15Å) was performed at the 3.6m CFHT with the MOS multislit spectrograph and at the 4.2m William Herschel Telescope (see M^cHardy *et al.* 1996 for details). Spectra were obtained within a contiguous region containing 73 X-ray sources above the flux limit of 2×10^{-15} erg cm $^{-2}$ s $^{-1}$ (0.5-2 keV). The survey region was largely defined by the positioning of the MOS fields and did not include some areas at large off-axis angles. Spectra were obtained of most objects of stellar appearance and $R < 22.5$ mag in the error circles, irrespective of other possible counterparts, in an attempt to identify all the X-ray sources which could be QSOs. The spectra of $R=22.5$ mag objects were of sufficient signal/noise (≈ 10) to identify typical QSO broad emission lines. In general, optical colours were not used to select candidates for spectroscopic observations in cases where two or more candidates existed, in order not to bias the identifications. In 9 of the 32 error circles in which QSOs were found a second object of $R \lesssim 22.5$ mag was also present. In 3 cases the second object had a stellar appearance. Spectra were obtained of 2 of the 3 stel-

lar objects, showing them to be normal Galactic stars. In all three cases the QSO was taken as the counterpart since (a) the QSO was nearer the error circle centre and (b) if all the X-ray flux was assumed to come from the star, its X-ray/optical flux ratio fell beyond the range found for stars of the same stellar type in the EMSS by Stocke *et al.* (1991). In six cases the second object was a faint galaxy, and since in five of them the QSO was nearest the error circle centre, and the X-ray/optical flux ratios of the QSO fell within the range found in the EMSS for AGN, it was taken as the counterpart. In one case (object 37) a faint galaxy of $R=22.5$ mag is 2 arcsec from the error circle centre and the QSO is 7.3 arcsec away. Since the total number of unrelated galaxies in all 32 QSO error circles, predicted from the optical counts of Metcalfe *et al.* (1991), is 8 at $R<22$ mag and 13 at $R<22.5$ mag, we have assumed that all these six galaxies are unrelated to the X-ray emission.

In 2 of the 32 X-ray sources another point X-ray source is closer than 1 arcmin. In these cases the X-ray source centroid positions produced by the source detection algorithm were slightly distorted and the correct positions were determined by an inspection of the X-ray image and overlaying the X-ray and optical images. In one case both sources (sources 29 and 154) are identified with QSOs 50 arcsec apart, but at different redshifts. In the other case (source 23) the QSO, at a redshift of $z=0.97$, and a narrow emission line galaxy at a redshift of $z=0.18$, are separated by only 20 arcsec. The peak of the X-ray emission lies nearest the QSO, and we have ignored the contribution from the narrow emission line galaxy. The X-ray/optical position offsets have been investigated omitting these three sources (numbers 23, 29 and 154) and splitting the sample into two flux ranges, with equal numbers of QSOs in each range. The mean position error for bright QSOs with flux $>8 \times 10^{-15}$ erg cm $^{-2}$ s $^{-1}$ (0.5-2 keV) was 3.0 arcsec (and within 5 arcsec for 95% of them), and for faint QSOs with flux $< 8 \times 10^{-15}$ erg cm $^{-2}$ s $^{-1}$ (0.5-2 keV) it was 5.2 arcsec (and within 10 arcsec for 95% of them), confirming the error circle size.

The 32 X-ray sources (out of a total of 73) with counterparts having at least one emission line of FWHM >1000 km s $^{-1}$ have been included in this analysis. Reliable redshifts from two or more emission lines were obtained for 90% of the QSOs. Eight sources out of 73 (11% of the total) were unidentified. The error circles of three of these contain galaxies of $R \approx 21-22$ mag with spectra of insufficient quality to classify them. The remaining five error circles are blank to $R=23$ mag, and deeper imaging has revealed only faint galaxies. We have assumed that the unidentified sources contain the same fraction of QSOs as the identified sources at the same flux and reduced the sky area as a function of flux by the fraction of all sources above each flux that have been identified. The corrected sky area is listed in Table 1. Since the unidentified sources are not among the brightest sources in the survey, and the QSO fraction of the identified sources falls with flux, the correction for incompleteness is not large. It is the equivalent of assuming 3 of the 10 unidentified sources are QSOs, in addition to the 32 identified QSOs. In practice, this correction may be too large, since QSOs, with their strong, broad emission lines, are the easiest class of X-ray source to identify.

3 ANALYSIS

3.1 X-ray spectra and the EMSS

Galactic absorption in the direction of this field is uniform and low ($N_H=6.5 \times 10^{19}$ cm $^{-2}$, Branduardi-Raymont *et al.* 1994). The small variations in the Galactic column density ($\sim 2 \times 10^{19}$ cm $^{-2}$) will have negligible effect on the flux at energies >0.5 keV, as used here. Thus ROSAT PSPC count rates were converted to 0.5-2 keV fluxes assuming a fixed column density of 6.5×10^{19} cm $^{-2}$ and a power law spectrum of energy index 1. The conversion factor was 1.1×10^{-11} erg cm $^{-2}$ s $^{-1}$ (ct s $^{-1}$) $^{-1}$. Romero Colmenero *et al.* (1996) have shown that a power law is a good description of most ($\approx 75\%$) of the spectra of the QSOs in this survey. The mean spectral index in the 0.1-2 keV band, ignoring the brightest ten QSOs, is 0.96 ± 0.03 . If all QSOs are summed into an average spectrum, the mean spectral index is 1.21 ± 0.03 (and is dominated by the brightest few QSOs) and the conversion factor used above would change by $<1\%$.

The ROSAT survey was analysed in combination with the EMSS survey of Stocke *et al.* (1991). The EMSS survey defined the low redshift X-ray luminosity function (XLF) and the high luminosity part of the high redshift XLF. In order to combine the two surveys, the ROSAT fluxes were converted to the *Einstein* 0.3-3.5 keV band via a constant conversion factor of 1.8. This factor is accurate to within 10% for simple power law spectra of energy index 0.3-2, assuming zero absorption intrinsic to each source (see Section 3.4 for the results of using a different conversion factor). All but one of the QSO spectral indices observed in the ROSAT sample are consistent with lying within this range (Romero Colmenero *et al.* 1996, figure 1). The 427 EMSS QSOs (Stocke *et al.* 1991) were used together with the 21 'expected' QSOs of Maccacaro *et al.* (1991), to account for EMSS incompleteness. The EMSS AGN sample included 32 sources which have an ambiguous classification and/or are uncertain identifications (tables 8 and 10 of Stocke *et al.* 1991). The EMSS optical spectra of these objects generally showed evidence of high ionization levels ($[\text{OIII}] \geq [\text{OII}]$) but either the signal/noise was insufficient to detect a broad permitted line component, or there was no coverage of $\text{H}\alpha$. Spectra of higher resolution and higher signal/noise of some of these objects have been obtained by Fruscione & Griffiths (1991), Boyle *et al.* (1995) and Halpern, Helfand & Moran (1995). Whilst in some of the objects the X-ray emission may arise from star formation activity, many of them do have weak broad permitted lines and may thus harbour AGN. Until detailed spectroscopy is available for all these objects, we have included them all in the analysis. They are all at redshifts $z \leq 0.42$.

Similar objects have been detected in our ROSAT survey. Initial spectroscopy of the sixteen narrow emission line galaxies indicates that they are also probably a mixture of starburst and Seyfert galaxies, at redshifts $z \leq 0.59$ (M c Hardy *et al.* 1996). We determine the effect of including these objects in the ROSAT sample on the XLF analysis below.

3.2 Redshift, Luminosity and Flux Distributions

The redshift distribution of the QSOs in the ROSAT survey is shown as a solid line in Figure 1. The EMSS QSO

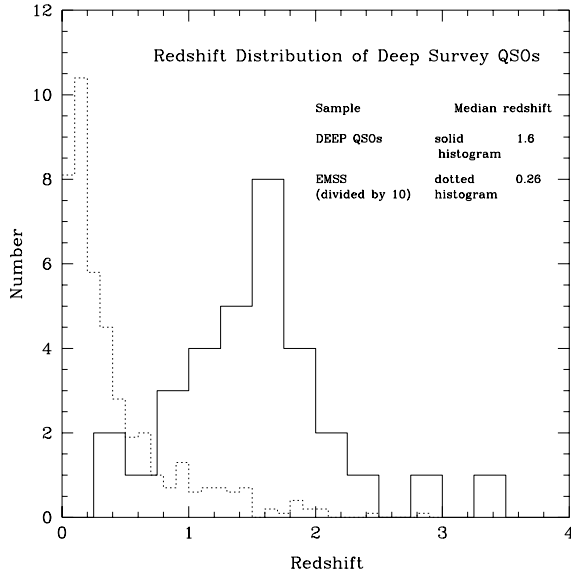


Figure 1. Redshift distribution $n(z)$ of the QSOs in the ROSAT Survey (solid line), and QSOs in the EMSS (dotted line). The ordinate is the number of objects per redshift interval of size 0.25. The EMSS numbers have been divided by a factor of 10 to fit on the plot.

redshift distribution is shown as a dotted line. The median ROSAT redshift is $z=1.6$, much higher than the median redshift in the EMSS of 0.3. There is a decline in the number of ROSAT QSOs starting at a redshift of $z \approx 1.8$. In Figure 2 the same ROSAT QSO redshift distribution is plotted, together with the redshift distribution of the sum of the ROSAT QSOs and narrow emission line galaxies (NELGs) as a dashed line. The difference in the redshift distributions of the two types of source immediately suggests that two different source populations are involved, even though the X-ray emission in some fraction of the NELGs may arise in Seyfert II AGN. We return to this point in the discussion.

The X-ray luminosity-redshift diagram is shown in Figure 3, for the ROSAT sample (solid symbols) and for the EMSS sample (open symbols). Also shown are lines of constant flux corresponding to the approximate limiting fluxes of the two surveys. The rest frame 0.3-3.5 keV luminosities were calculated assuming $H_0=50 \text{ km s}^{-1} \text{ Mpc}^{-1}$, $q_0=0.5$ and an X-ray spectral index of 1. This spectral index is the mean value for radio quiet QSOs in the EMSS (Wilkes & Elvis 1987). The ROSAT survey samples luminosities a factor ≈ 30 lower than the EMSS survey at redshifts $z > 1$. A QSO of luminosity $\sim 10^{44} \text{ erg s}^{-1}$, typical for nearby QSOs (Maccacaro *et al.* 1991), is detectable up to a redshift of $z=2$ in the ROSAT survey, and we thus expect the ROSAT survey to help define the low luminosity, high redshift part of the luminosity function. At redshifts $z > 1.5$ there are approximately equal numbers of QSOs in the ROSAT survey as in the EMSS, but at very different luminosities.

The QSO integral number-flux relation, or $\log(N)$ - $\log(S)$ diagram, is shown in Figure 4a. The ROSAT QSO fluxes have been converted to the *Einstein* 0.3-3.5 keV band using the conversion factor of 1.8 described above. A correction has also been made for the QSOs at bright fluxes

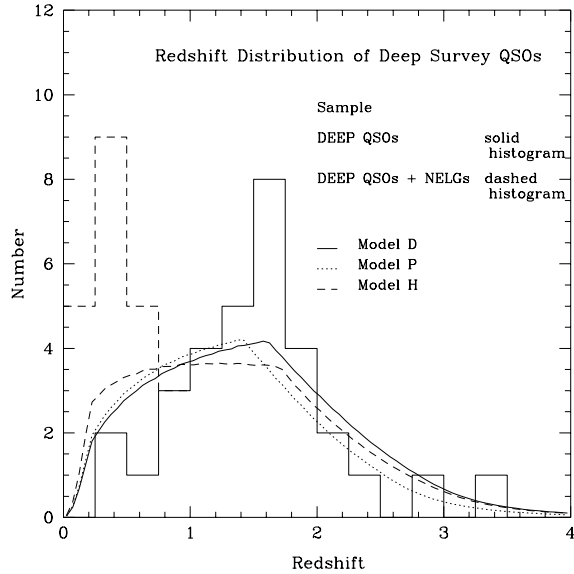


Figure 2. Redshift distribution of the QSOs in the ROSAT survey as in Figure 1, together with the sum of the ROSAT QSOs and narrow emission line galaxies (NELGs) as a dashed line, and the predicted $n(z)$ of models D, P & H. (see text). Note that the dashed histogram follows the solid histogram exactly at $z > 0.75$, because there are no nelgs at $z > 0.75$.

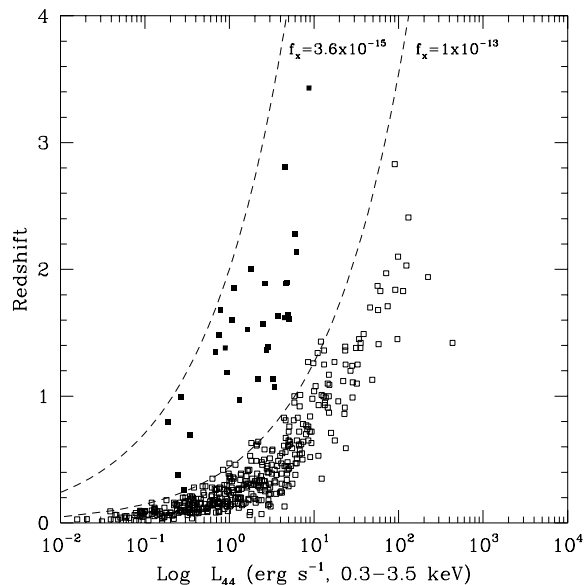


Figure 3. X-ray luminosity-redshift diagram for ROSAT QSOs (solid symbols) and EMSS QSOs (open symbols). Lines of constant flux corresponding to the approximate survey flux limits are also shown.

missed in the ROSAT pencil-beam survey because of their rarity on the sky. This small correction was 6 deg^{-2} , corresponding to one QSO predicted in the survey area (at fluxes of $> 9 \times 10^{-14} \text{ erg cm}^{-2} \text{ s}^{-1}$, 0.3-3.5 keV). The surface density of QSOs at the flux limit of the ROSAT survey is $230 \pm 40 \text{ deg}^{-2}$, the largest measured for a QSO survey at any wavelength. The counts are in good agreement with those

of Boyle *et al.* (1994) (shown as filled circles in Figure 4a), except for a slight excess in our field at a flux $\approx 2 \times 10^{-14}$ erg $\text{cm}^{-2} \text{s}^{-1}$.

A break in the integral QSO counts of Figure 4a is apparent at a flux $\approx 2 \times 10^{-14}$ erg $\text{cm}^{-2} \text{s}^{-1}$ (0.3-3.5 keV). This break can also be clearly seen in the differential $\log(N)$ - $\log(S)$ relation of Figure 4b. The slope of the QSO $\log(N)$ - $\log(S)$ relation, measured from the 21 QSOs fainter than this flux, is -0.3 ± 0.4 . The slope was measured from a minimum χ^2 fit to the differential counts. It is significantly flatter than the slope of -1.61 ± 0.06 measured at bright fluxes in the EMSS QSO sample by Della-Ceca *et al.* (1992), at $> 3\sigma$ significance. The break in the QSO $\log(N)$ - $\log(S)$ relation occurs at approximately the same flux as the break in the counts of all X-ray sources measured by Branduardi-Raymont *et al.* (1994). Since QSOs account for $\approx 80\%$ of all X-ray sources at the break flux (Shanks *et al.* 1991, M^cHardy *et al.* 1996), it is the QSOs which are responsible for this break. Although there is no overlap in the flux range of the QSOs in the ROSAT survey and the EMSS, the bright ROSAT QSO counts are consistent with a direct extrapolation of the EMSS QSO counts, given by the dotted line in Figure 4a. However, since there are only eleven ROSAT QSOs at fluxes brighter than the break, the count slope and normalisation at bright fluxes are not well constrained.

3.3 The X-ray Luminosity Function

3.3.1 The binned Luminosity Function

An initial estimate of the differential X-ray luminosity function (XLF) was obtained by binning the QSOs from the combination of the two surveys in redshift and luminosity. We used the $1/V_a$ statistic of Avni and Bachall (1980) as described by Maccacaro *et al.* (1991). The XLF at five redshift intervals is shown in Figure 5a for $q_0 = 0.5$ and Figure 5b for $q_0 = 0$. The XLF is plotted here per logarithmic luminosity bin (although it is defined below per linear luminosity bin) so that pure luminosity evolution will produce a simple shift along the luminosity axis. K-corrections were unity, assuming a spectral index of 1. Error bars have been estimated assuming Poissonian errors based on the number of QSOs in each bin. All points represent at least two QSOs. Upper limits to the XLF have been plotted for some bins containing one or zero QSOs. The upper limit was set at 3 QSOs, corresponding to 80% confidence. Where there was one QSO detected, the position of the symbol represents the value of Φ given by the single QSO, and the upper limit represents < 3 QSOs. The lowest three redshift intervals are those used by Boyle *et al.* (1994) and give a constant width in $\log(1+z)$. The remaining redshift intervals explore the XLF behaviour at the redshift $z \approx 2$ where a halt or slowing of the pure luminosity evolution is found in the optical surveys of Boyle *et al.* (1991), although because these binned XLF estimates do not take into account any evolution occurring within each bin, they are not used to quantify the detailed XLF evolution.

The XLF has a two power law form at all redshifts where there are enough QSOs to provide a good measurement (up to $z=2.2$). Comparison with Figure 6 of Maccacaro *et al.* (1991) shows that the addition of the ROSAT data has

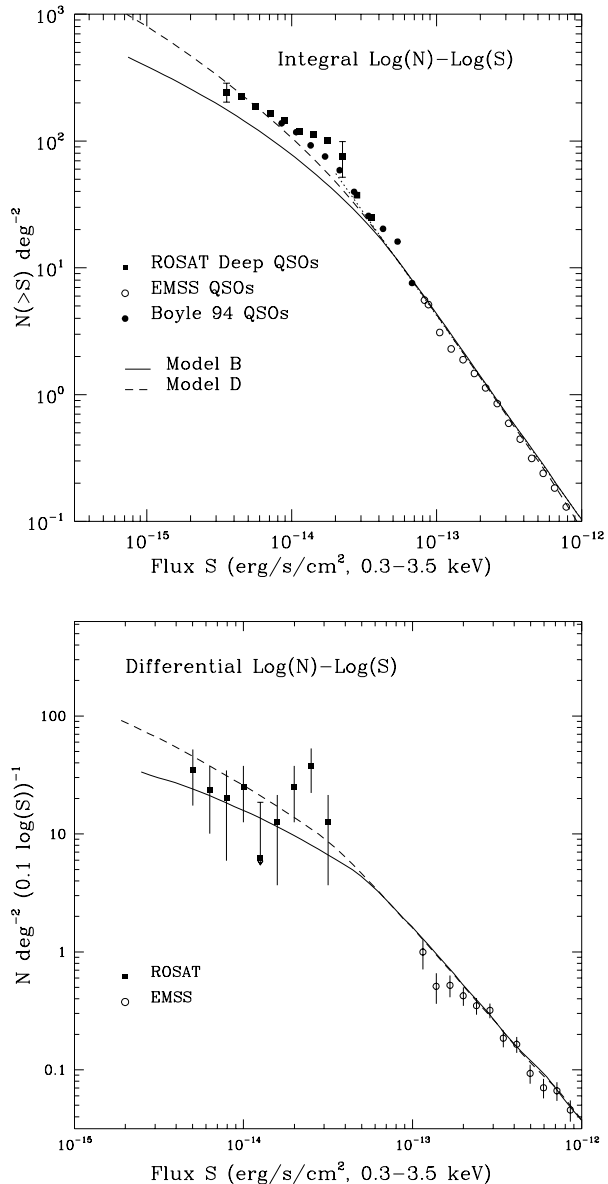


Figure 4. (a) Integral $\log(N>S)$ - $\log(S)$ relation for QSOs in the ROSAT deep survey (filled squares), EMSS AGN (open circles), and Boyle *et al.* (1994) ROSAT survey (filled circles, shifted by 0.03 in $\log(S)$ for clarity). The dotted line shows the extrapolation of the best fit EMSS slope of 1.61 to fainter fluxes. Models B (solid line) and D (dashed line) are described in the text. (b) the same data as in (a) are plotted, but in independent, differential bins.

extended the measurement of the XLF to low luminosities (lower than the break luminosity) at redshifts $0.4 < z < 2.2$. Our measurement of the XLF also extends to lower luminosities than the ROSAT surveys of Boyle *et al.* (1994) and Page *et al.* (1996). As noted in previous investigations, the general form of the evolution of the XLF is of luminosity evolution, in which the shape of the XLF and the number of QSOs are conserved with redshift, but the characteristic QSO luminosity increases with redshift. For $q_0=0.5$, it is clear from Figure 5a that the luminosity evolution which appears to be a good description at low redshifts does not

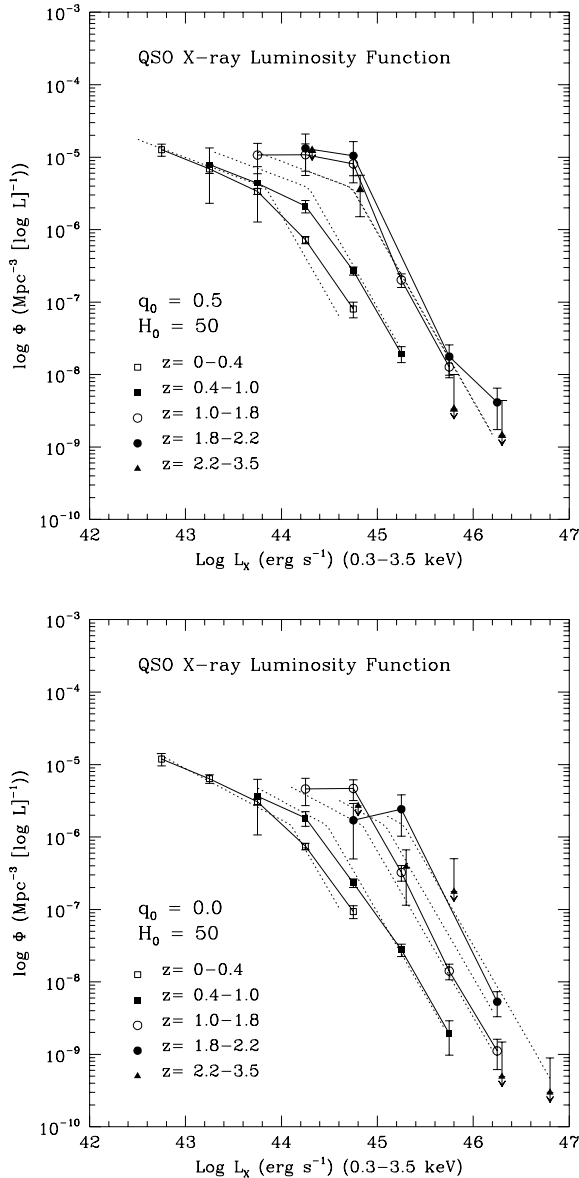


Figure 5. Binned $1/V_a$ estimates of the XLF in different redshift shells, from the combined ROSAT and EMSS samples. Upper limits are denoted by arrows. Some points have been moved slightly by 0.05 in $\log(L_X)$ for clarity. See the text for details of the models. (a) For $q_0=0.5$. Dotted lines are from model B. (b) For $q_0=0.0$. Dotted lines are from model D.

continue to high redshifts. The XLFs at redshifts $1.8 < z < 2.2$ and $2.2 < z < 3.5$ are identical, within the measurement errors, to that at $1 < z < 1.8$.

The small number of QSOs detected at $z > 2.2$ does not indicate a further change in the evolutionary behaviour of the XLF beyond the halt in the luminosity evolution at $z \approx 1.8$, despite the depth of the survey. The filled triangles at $L = 10^{44.25} \text{ erg s}^{-1}$ (Figure 5a) and $L = 10^{44.75} \text{ erg s}^{-1}$ (Figure 5b) represent upper limits of < 3 QSOs where none were detected. The upper limits are consistent with the XLF at lower redshifts $1.8 < z < 2.2$.

The dotted lines in Figure 5a represent the best fit model of the XLF (model B). At redshifts of $1 < z < 2.2$ and

luminosities of $10^{44.5} < L < 10^{45} \text{ erg s}^{-1}$ there is a small excess of QSOs observed over the model prediction. This excess is not statistically significant; 2.5 are predicted and 5 were observed, a not unlikely 11% probability. This small excess is also visible in the $n(z)$ data of Figure 2, where the excess of $\approx 3-4$ QSOs over the 4 QSOs expected at $1.5 < z < 1.75$ has $\approx 5\%$ chance of occurring in a random distribution (again not unlikely given the 13 bins of Figure 2), and at fluxes of $2-3 \times 10^{-14} \text{ erg cm}^{-2} \text{ s}^{-1}$ in the $\log(N)-\log(S)$ relation of Figure 4b. The presence of large scale structure is not required to explain this excess.

For $q_0=0$ (Figure 5b), there is much less evidence for a slowing of the luminosity evolution. The $2.2 < z < 3.5$ XLF seems to lie at approximately the same values as the $1.8 < z < 2.2$ XLF, but there are only 5 QSOs contributing to the $2.2 < z < 3.5$ XLF, and the measurement errors are large. The apparent change in the slope of the low luminosity part of the $q_0=0$ XLF with redshift (at luminosities less than the break luminosity) is due to the small number of QSOs at these luminosities at $z > 1.8$. The observations at $z > 1.8$ are consistent within the measurement errors with the slope at low redshifts.

3.3.2 Fitting an evolutionary model

To derive more quantitative information, we used the maximum likelihood method of Marshall *et al.* (1983) to obtain the best-fit model of the shape of the XLF and its evolution. We have investigated pure luminosity evolution models, guided by the appearance of the XLF in Figure 5, but not density evolution models. The level of density evolution, in which the XLF retains its shape but changes normalisation with redshift, has been shown by Boyle *et al.* (1988) to be at least 60 times slower than the corresponding luminosity evolution for high luminosity optically selected QSOs. Following Maccacaro *et al.* (1991), Della-Ceca *et al.* (1992) and Boyle *et al.* (1993, 1994) we define the differential XLF as a two power law function with a break at luminosity L_z^* :

$$\Phi(L) = \frac{dN}{dLdV} = \frac{\Phi^*}{L_{z44}^*} \left(\frac{L_{44}}{L_{z44}^*} \right)^{-\alpha_1} \quad (L \leq L_z^*)$$

$$\Phi(L) = \frac{dN}{dLdV} = \frac{\Phi^*}{L_{z44}^*} \left(\frac{L_{44}}{L_{z44}^*} \right)^{-\alpha_2} \quad (L > L_z^*)$$

The luminosities are in units of $10^{44} \text{ erg s}^{-1}$ (0.3-3.5 keV). The slopes at low and high luminosities are α_1 and α_2 , and the XLF normalisation is Φ^* . The normalisation is slightly different from that used by Boyle *et al.* (1993,1994):

$$\Phi^* = \Phi_{B94}^* L_{z44}^{*1-\alpha_1}$$

We assumed a pure luminosity power law form for the evolution of the XLF with a redshift cutoff z_{cut} :

$$L_z^*(z) = L_0^*(0)(1+z)^k \quad (z < z_{cut})$$

$$L_z^*(z) = L_0^*(0)(1+z_{cut})^k \quad (z \geq z_{cut}).$$

In this model the luminosity evolution continues up to redshift z_{cut} , but beyond this redshift the luminosity function is invariant with redshift. Evolutionary models both with and without this redshift cutoff were investigated. Exponential luminosity evolution models were not investigated because

they have been found to be a poor description of QSO X-ray evolution by e.g. Boyle *et al.* (1993).

The number of free parameters to be constrained by the maximum likelihood fit was four or five; α_1 , α_2 , L_0^* , k , and in some models, z_{cut} . The normalisation Φ^* was determined by the total number of QSOs in the samples, and was not a free parameter.

To estimate the goodness-of-fit of the model to the data, the 2-dimensional Kolgorov-Smirnov (2D KS) test of Fasano & Franceschini (1987), as implemented by Press *et al.* (1992), was used. The test was performed over the complete range of redshifts and luminosities available, $0 < z < 4$ and $10^{42} < L < 10^{47}$ erg s⁻¹. Having obtained a good fit, errors on the parameters were determined from the increase ΔS in negative log(likelihood) away from the minimum value, allowing all free parameters to vary. The value of ΔS was chosen according to the number of free parameters to give 68% confidence limits (Lampton, Margon & Bowyer 1976).

3.4 Results

The results of the maximum likelihood fits and 2D KS tests are listed in Table 2. For $q_0=0.5$, the power law luminosity evolution model with no redshift cutoff in the evolution is unacceptable at the 1 per cent level (model A). Introducing the cutoff makes the model acceptable at >20 per cent probability (model B). The best value for the redshift cutoff is $z_{cut}=1.41$ (+0.4,-0.17, at 68% confidence). The value of the evolution index is $k=2.97$ (+0.19,-0.34). These best fit values of z_{cut} and k are in excellent agreement with those found by Page *et al.* (1996) ($z_{cut}=1.42$, $k=2.94$), and consistent with those found by Boyle *et al.* (1994) based on ROSAT data alone ($z_{cut}=1.6$, $k=3.25$).

For $q_0=0$, an acceptable fit is found for the power law luminosity evolution model at the 5 per cent confidence level with or without a redshift cutoff (models D and C). The introduction of a redshift cutoff into the model gives a best fit value of $z_{cut}=1.6$ and increases the best fit value of the evolution index from $k=2.46$ (+0.11,-0.14) to $k=3.0$ (+0.27,-0.4).

The ROSAT QSO log(N)-log(S) relation of Page *et al.* (1996) extended to brighter fluxes than ours and overlapped with the EMSS relation. They found that although the slopes of the two relations were consistent (and thus that the EMSS is probably reasonably complete), there was an offset in flux between the two relations. This offset could be removed if a ROSAT 0.5-2 keV to *Einstein* 0.3-3.5 keV bandpass conversion factor of 1.47 was adopted instead of the value of 1.8 given by a spectral index of 1. We have investigated the effect of using this lower value in models I to L. There is no effect on which models are acceptable, although the probability of both q_0 models is smaller, and the model parameters change very little (see Table 2).

4 DISCUSSION

4.1 Evolution models

We have only considered pure luminosity evolution models. Pure density evolution would not match the binned XLF estimates of Figure 5.

For both $q_0=0.5$ and $q_0=0$, pure luminosity evolution is a good description of the low redshift XLF evolution. The evolution can be characterized as a power law in $(1+z)$, i.e. $L_X \propto (1+z)^{3.0(+0.19,-0.34)}$. For $q_0=0.5$, this evolution halts at a redshift of 1.4 (+0.4,-0.17), and we detect no further change in the XLF up to $z \sim 3$. The log(N)-log(S) prediction of this model (model B) is shown as a solid line in Figure 4. Figure 4a shows that the model predicts a lower number of ROSAT QSOs than were observed, but the prediction of the total number of QSOs in the ROSAT survey is only 1.5σ below the total number observed. The integral log(N)-log(S) plot can be misleading since the data points are not independent; the model is consistent with the differential log(N)-log(S) relation shown in Figure 4b. In three surveys (this work, Page *et al.* 1996 and the ROSAT data of Boyle *et al.* 1994) it has now been found that, for $q_0=0.5$, the luminosity evolution of the X-ray QSO XLF halts at a redshift of $z=1.4-1.6$ and the evolution parameter k lies in the range $k=2.9-3.25$ (where the comparison is with the values obtained using a ROSAT to EMSS bandpass conversion factor of 1.8).

For $q_0=0$, although a halt in the luminosity evolution is not required by the data, when it is included (model D), the value of z_{cut} is 1.6, again similar to the values found by Page *et al.* (1996) (1.82) and Boyle *et al.* (1994) (1.79 for ROSAT data alone). The evolution parameter k is 3.0, 2.9 and 3.3 in this work, Page *et al.* and Boyle *et al.* respectively. The log(N)-log(S) prediction of model D, shown as a dashed line in Figures 4a and 4b, matches the observed log(N)-log(S) relations and predicts more faint QSOs than model B (for which q_0 is 0.5). The $n(z)$ prediction of model D, using the normalisation given in Table 2, is shown in Figure 2. The prediction matches the observed QSO $n(z)$ distribution.

4.2 Errors of derived parameters

Before discussing in detail the different results of ROSAT, EMSS and optical surveys, we examine the methods used to determine the size of the errors of the parameters describing the shape and evolution of the XLF, since these are crucial in interpreting different results. We estimated the errors by stepping each parameter away from the best-fit value, re-minimizing S (where $S=-2\ln(L)$ and L is the likelihood function), and finding the parameter value which gave an increase in S of ΔS above the minimum. The appropriate value of ΔS to use is a function of the confidence level required and the number of free parameters (Lampton, Margon and Bowyer 1976), since the error values obtained are a projection of the multi-dimensional confidence region on to each parameter axis in turn. For 68% (90%) confidence and 4 free parameters, we used $\Delta S=4.7$ (7.78); for 5 free parameters, we used $\Delta S=5.9$ (9.2). Since the errors on different parameters are correlated, a parameter value at the edge of a confidence region as defined here will not in general be consistent with the full confidence region of other parameters, but only a smaller region. However, our definition of the confidence region does give an estimate of the total

Table 2. XLF and evolution parameters, EMSS+ROSAT data

| Model | Sample(s) | q_0 | evolution | α_1 | α_2 | L_{044}^* § | k | z_{cut} | Φ_* † | P_{KS} ‡ |
|-------|--------------------|-------|-----------------------|------------------------|------------------------|------------------------|------------------------|------------------------|------------|------------|
| A | EMSS + ROSAT QSOs | 0.5 | $(1+z)^k$ | 1.55 | 3.26 | 0.51 | 2.21 | - | 1.28 | 0.005 |
| B | " | 0.5 | $(1+z)^k (< z_{cut})$ | $1.50^{+0.20}_{-0.24}$ | $3.32^{+0.17}_{-0.12}$ | $0.40^{+0.17}_{-0.08}$ | $2.97^{+0.19}_{-0.34}$ | $1.41^{+0.40}_{-0.17}$ | 1.64 | 0.21 |
| C | " | 0.0 | $(1+z)^k$ | $1.71^{+0.11}_{-0.21}$ | $3.29^{+0.12}_{-0.17}$ | $0.81^{+0.18}_{-0.25}$ | $2.46^{+0.11}_{-0.14}$ | - | 0.63 | 0.12 |
| D | " | 0.0 | $(1+z)^k (< z_{cut})$ | $1.58^{+0.22}_{-0.25}$ | $3.31^{+0.18}_{-0.13}$ | $0.50^{+0.30}_{-0.12}$ | $3.03^{+0.27}_{-0.40}$ | $1.61^{+0.37}_{-0.27}$ | 1.07 | 0.045 |
| E | EMSS + ROSAT QSOs | 0.5 | $(1+z)^k$ | 1.72 | 3.32 | 0.6 | 2.31 | - | 1.00 | 0.010 |
| F | + ROSAT NELGs | 0.5 | $(1+z)^k (< z_{cut})$ | $1.65^{+0.24}_{-0.18}$ | $3.30^{+0.34}_{-0.09}$ | $0.41^{+0.42}_{-0.06}$ | $2.97^{+0.24}_{-0.33}$ | $1.41^{+0.39}_{-0.21}$ | 1.52 | 0.19 |
| G | " | 0.0 | $(1+z)^k$ | $1.84^{+0.12}_{-0.12}$ | $3.30^{+0.23}_{-0.11}$ | $0.88^{+0.26}_{-0.22}$ | $2.46^{+0.24}_{-0.14}$ | - | 0.53 | 0.17 |
| H | " | 0.0 | $(1+z)^k (< z_{cut})$ | $1.78^{+0.19}_{-0.18}$ | $3.29^{+0.21}_{-0.10}$ | $0.64^{+0.29}_{-0.21}$ | $2.79^{+0.55}_{-0.14}$ | $1.70^{+0.36}_{-0.35}$ | 0.76 | 0.25 |
| I | EMSS + ROSAT QSOs | 0.5 | $(1+z)^k$ | 1.55 | 3.26 | 0.56 | 2.28 | - | 1.27 | 0.005 |
| J | S(0.3-3.5 keV)= | 0.5 | $(1+z)^k (< z_{cut})$ | 1.50 | 3.30 | 0.40 | 2.97 | 1.37 | 1.63 | 0.24 |
| K | 1.47x S(0.5-2 keV) | 0.0 | $(1+z)^k$ | 1.64 | 3.08 | 0.70 | 2.20 | - | 0.83 | 0.053 |
| L | " | 0.0 | $(1+z)^k (< z_{cut})$ | 1.59 | 3.25 | 0.56 | 2.79 | 1.66 | 0.97 | 0.03 |
| M | EMSS only | 0.5 | $(1+z)^k$ | $1.71^{+0.22}_{-0.25}$ | $3.33^{+0.89}_{-0.24}$ | $0.78^{+1.1}_{-0.23}$ | $2.18^{+0.23}_{-0.33}$ | - | 0.77 | 0.07 |
| N | " | 0.5 | $(1+z)^k (< z_{cut})$ | $1.62^{+0.20}_{-0.29}$ | $3.31^{+0.24}_{-0.27}$ | $0.50^{+0.24}_{-0.16}$ | $2.80^{+0.31}_{-0.28}$ | $1.41^{+0.6}_{-0.21}$ | 1.17 | 0.29 |
| O | " | 0.0 | $(1+z)^k$ | $1.65^{+0.20}_{-0.19}$ | $3.19^{+0.32}_{-0.10}$ | $0.63^{+0.31}_{-0.14}$ | $2.46^{+0.24}_{-0.13}$ | - | 0.92 | 0.05 |
| P | " | 0.0 | $(1+z)^k (< z_{cut})$ | $1.59^{+0.24}_{-0.25}$ | $3.22^{+0.29}_{-0.14}$ | $0.45^{+0.5}_{-0.12}$ | $3.03^{+0.23}_{-0.45}$ | $1.42^{+0.8}_{-0.18}$ | 1.22 | 0.14 |

§ Break luminosity at $z=0$ in units of 10^{44} erg s^{-1} (0.3-3.5 keV)† XLF normalisation in units of 10^{-6} Mpc $^{-3}$ (10^{44} erg s^{-1}) $^{-1}$

‡ 2D KS probability

Errors, where quoted for models which are a good fit, are at 68% confidence.

range of values each parameter could take, taking into account the errors on all the other parameters. The errors are in general non-linear and non-symmetric, so the 90% confidence errors for many parameters are only slightly larger than the 68% confidence errors. As a consistency check, we noted the values of the 2D KS probability P_{KS} as z_{cut} was stepped away from the best-fit value of 1.41 in model B, and S re-minimized at each step. P_{KS} fell below 0.1 (i.e. 90% probability) at 1.41 (+0.5,-0.4), in approximate agreement with the $\Delta S=9.2$ (90%) values of +0.5,-0.21 and $\Delta S=5.9$ (68%) values of +0.4,-0.17.

Some previous QSO LF investigations (Page *et al.* 1996; Boyle *et al.* (1993,1994); Boyle, Shanks & Peterson 1988) have used $\Delta S=1$ when models have had 4 or more free parameters. As noted by Boyle, Shanks & Peterson (1988), $\Delta S=1$ is only strictly valid for the case of one parameter taken in isolation (e.g. the confidence region for the evolution parameter k assuming zero error on the XLF shape and redshift cutoff). For our combined ROSAT+EMSS surveys and models, a value of $\Delta S=1$ gives errors smaller by factors varying from 2 to 5 compared with the higher ΔS values used here. Boyle *et al.* (1994) note that a better estimate of their parameter errors may be obtained from the variations in parameter values from model to model rather than the $\Delta S=1$ values. A comparison can also be made with the error estimates of Maccacaro *et al.* (1991) and Della-Ceca *et al.* (1992), who analysed the EMSS using a different method from that used here. Their 68% confidence error estimates of $k=2.56\pm 0.17$, derived from the error on the V/V_{max} statistic, are in reasonable agreement with our analysis of the same data (model O) which gives $k=2.46$ (+0.24,-0.13).

4.3 ROSAT and EMSS X-ray QSO evolution

Previous authors have emphasized the different values obtained for the pure luminosity evolution parameter k from the EMSS and ROSAT surveys. The EMSS value of $k=2.56\pm 0.17$ (for $q_0=0$; Della-Ceca *et al.* 1992) appears significantly lower than the ROSAT value of 3.34 ± 0.1 (Boyle *et al.* 1994) and the combined ROSAT+EMSS values of 2.9-3.0 (this paper, Page *et al.* 1996 and Boyle *et al.* 1994). Franceschini *et al.* (1994) offered a possible explanation by analysing a subset of the EMSS data, restricted to fluxes $> 2.6 \times 10^{-13}$ erg $cm^{-2} s^{-1}$, and finding a best-fit value of $k=3.27$ (assuming an X-ray spectral index of one). They suggested that the EMSS might be incomplete at faint fluxes.

However, it is important to compare results from the same assumed evolutionary model. Our result (for the combined ROSAT+EMSS data and $q_0=0$) that the value of k increased significantly when a redshift cutoff was introduced into the model prompted us to re-analyse the EMSS data including a redshift cutoff. This model was not considered by Maccacaro *et al.* (1991) or Della-Ceca *et al.* (1992). The results are given in Table 2, models M-P. For $q_0=0$ and no redshift cutoff (model O), $k=2.46$ (+0.24,-0.13), consistent with the previous EMSS results. When a redshift cutoff is introduced, the evolution index increases to $k=3.03$ (+0.23,-0.45), and the redshift cutoff value is $z_{cut}=1.4$ (+0.8,-0.18) (model P). The large errors are an indication that model P is over-complicated and the EMSS data do not require a redshift cutoff; nevertheless, if a redshift cutoff is included in the model, the EMSS data are best fit with a high value of k , consistent with the results from combined EMSS+ROSAT surveys, and the ROSAT data alone of Boyle *et al.* (1994). In addition, this model, derived from the EMSS data alone,

predicts a redshift distribution for the ROSAT survey which is consistent with the ROSAT data (see Figure 2). A similar increase in the best-fit EMSS value of k when a redshift cutoff is included, from $k=2.18$ to $k=2.80$, is found for $q_0=0.5$ (models M and N).

The converse is also in general true. If a redshift cutoff is *not* included, the combined ROSAT+EMSS surveys of this paper, Page *et al.* (1996) and Boyle *et al.* (1994) give consistent values of $k=2.46$ (+0.11,-0.14), 2.66 ± 0.08 and 2.63 ± 0.1 respectively ($q_0=0$). Ciliegi *et al.* (1995) also found relatively low values of the evolution parameter from combined ROSAT and EMSS samples, with no redshift cutoff in their model. The ROSAT data alone of Boyle *et al.* (1994) give $k=2.66\pm 0.1$. Boyle *et al.* (1993), with a smaller number of ROSAT QSOs, found a value of $k=2.75\pm 0.1$ for their combined ROSAT+EMSS survey and $k=2.9$ for the ROSAT data alone. The value of $k=2.75\pm 0.1$ is consistent with the EMSS value of 2.56 ± 0.17 at the 68% confidence level, and the addition of more ROSAT QSOs (Boyle *et al.* 1994) has resulted in a new value of 2.63 ± 0.1 .

The reason for the increase in the EMSS evolution parameter when a redshift cutoff is introduced is that many of the EMSS QSOs are at redshifts higher than the redshift $z\approx 1.6$ where the evolution halts or slows (see Figure 3). The evolution parameter is insensitive to the numerous low redshift $z\sim 0.2$ EMSS QSOs, so if a single value of k is assumed to apply at all redshifts, with no redshift cutoff, the high redshift QSOs weight the best fit of a straight line in the $\log(L_z^*)-\log(1+z)$ plane to a flatter slope, or a lower value of k .

Thus, although the EMSS contains too few high redshift QSOs to constrain the redshift cutoff, the EMSS data are consistent with an evolution index of $k=3.0$, higher than the value of $k=2.56$ found by Maccacaro *et al.* (1991) and Della Ceca *et al.* (1992), and consistent with that found from recent ROSAT surveys. In general, four X-ray surveys (the EMSS and those of Boyle *et al.* (1994), Page *et al.* (1996) and this work) give consistent results for the evolution index: $k=2.8-3$, with a redshift cutoff of $z_{cut}=1.4-1.8$. There are, however, two caveats to this statement. First, none of the surveys is completely independent, since all incorporate the EMSS. Boyle *et al.* (1994) found a slightly higher value of $k=3.2-3.3$ from ROSAT data alone (with a fixed XLF shape). Secondly, Boyle *et al.* (1994) also required more complicated models (e.g. a ‘polynomial’ pure luminosity evolution model) in order to achieve statistically acceptable fits to the combined ROSAT and EMSS data, although each dataset could be fit separately by the simpler luminosity evolution models used here. A possible explanation is investigated in section 4.5.

The high value of the EMSS evolution parameter found by Franceschini *et al.* (1994) was obtained with a redshift cutoff fixed at $z_{cut}=2.5$ and a bright flux limit. The bright flux limit will have reduced the number of high redshift QSOs somewhat; the combination of this factor and the redshift cutoff (although it has a high value) may have partly produced the increase in the evolution parameter, rather than incompleteness in the EMSS, as suggested by Franceschini *et al.* (1994).

4.4 X-ray and optical QSO evolution

Comparing X-ray and optically selected QSO surveys, the X-ray evolution index ($k=2.97+0.19,-0.34$) and redshift cutoff ($z_{cut}=1.4+0.4,-0.17$) found here for $q_0=0.5$ are both lower than that found by Boyle *et al.* (1991) ($k=3.45$, $z_{cut}=1.9$) from a combination of optical surveys. Although the values of z_{cut} are consistent at 68% significance, this is a general finding for all X-ray QSO surveys. These differences cannot arise from different sampling of redshift space assuming the simple evolution model used here; if the X-ray sampling and measurement errors produced a best-fit redshift cutoff at a lower redshift than the true value, then a higher value of the X-ray evolution index would be produced, not a lower value. However, recent optical surveys indicate that simple pure luminosity evolution may no longer be an adequate description of optical QSO evolution. Hewett *et al.* (1993), in an analysis of an independent optical survey, find that optical luminosity evolution slows down at a redshift of $z\sim 1.5$, and that it continues at a slower rate corresponding to $k\sim 1.5$ up to a redshift of $z\sim 3$. In addition, Hewett *et al.* (1993) and Miller *et al.* (1993) observe a change in shape of the optical luminosity function with redshift, such that the high luminosity slope is steeper at higher redshift. Neither of these effects are currently observed in X-ray samples.

4.5 Absorption and emission features in QSO X-ray spectra

The range of rest frame energies in the ROSAT and EMSS surveys is 0.3-3.5 keV for the EMSS at $z=0$, 2-8 keV for ROSAT at $z=3$, and 0.9-10.5 keV for the EMSS at $z=2$. The assumption of a mean QSO spectrum of a smooth power law of spectral index one is unlikely to be correct. Here we estimate how good that assumption is. These estimates do not include the details of the different instrumental responses, but rather provide an approximate estimate of the size of the effects.

Although the value of the mean spectral index ≈ 1 obtained from low resolution, low signal-to-noise X-ray spectra (typical of those from ROSAT surveys and the EMSS) is confirmed by detailed studies of brighter AGN (e.g. Nandra & Pounds 1994), the observed spectra contain emission lines and photoelectric absorption features. The potential effects are on the count rate to flux conversion factor, the ROSAT-*Einstein* bandpass conversion factor, and the K-correction. In practice, the effect on the count rate to flux conversion is negligible, as shown by the wide range of power law indices that have $<10\%$ effect (see section 3.1).

An absorption edge and fluorescent emission line (at a rest energy of 6.4 keV) due to highly ionized iron, together with scattered photons at higher energies (the ‘reflection bump’) have been found to be common in Seyfert I AGN (Nandra & Pounds 1994). The iron features are redshifted into the ROSAT band at $z>2.2$ and into the EMSS band at $z>0.9$. However, the typical iron line equivalent width of ≈ 200 eV would produce a change in the flux in the EMSS or ROSAT bands of $\leq 2\%$, small enough to ignore. The reflection bump, at rest energies >8 keV, will have a larger effect on ROSAT QSOs at $z>3$ and EMSS QSOs at $z>1.3$. For the highest redshift EMSS QSOs (at $z\sim 2.5$) the effect of the reflection bump would be to change the EMSS flux by $<10\%$.

However, EMSS QSOs at these redshifts are all of high luminosity ($>10^{45}$ erg s $^{-1}$), and there have been fewer detections of a reflection bump in high luminosity sources compared to lower luminosity AGN (e.g. Williams *et al.* 1992).

A more important feature has been detected in some ASCA AGN spectra. The ASCA spectral resolution has revealed what may be the strongest feature in the 0.4-6 keV band; OVII and OVIII absorption edges at 0.72 keV and 0.87 keV, known as ‘warm’ absorbers (e.g. Otani *et al.* 1996a, Fabian *et al.* 1994 and references therein). Otani *et al.* (1996b) found that six out of eight type 1 AGN, with luminosities of 10^{42} to 10^{45} erg s $^{-1}$, contain similar absorption features. The total absorption was $\approx 20\%$ of the 0.5-2 keV flux in all six objects, and was all within the 0.5-2 keV band. The fraction of AGN which exhibit such absorption features is not well known, although Nandra & Pounds (1994) found $\sim 50\%$ of their sample of 28 AGN to do so. We will estimate the worst-case systematic effect of all AGN containing a warm absorber. The effect on the ROSAT 0.5-2 keV to *Einstein* 0.3-3.5 keV passband conversion at zero redshift is to increase the factor from 1.8 to ≈ 2.0 , since a smaller fraction of the *Einstein* flux is absorbed. The size of this effect is similar to that required by Page *et al.* (1996) to match ROSAT and EMSS log(N)-log(S) relations, but in the opposite sense; Page *et al.* required a conversion factor of 1.47. At $z > 1.6$, the absorption features are redshifted out of the ROSAT band, but may effect the EMSS fluxes at energies below the carbon edge in the detector windows, given the modest energy resolution. Whilst the exact value of the conversion factor depends on the instrumental responses and resolutions, a value smaller than 1.8, perhaps ≈ 1.6 , may be required for some of our ROSAT QSOs. We have already shown, however, that decreasing the conversion factor from 1.8 to 1.47 (models I-J) has little effect on our results. The redshift-dependent effect of the warm absorber spectral feature may however help explain the ROSAT/EMSS log(N)-log(S) discrepancy of Page *et al.* (1996), and partly explain the poor fits found by Boyle *et al.* (1994) in their combined EMSS+ROSAT sample, with a much larger number of ROSAT QSOs than used here.

The effect of the warm absorbers on the K-correction in the ROSAT band would be to decrease the K-correction with increasing redshift from 1 at low redshifts to a minimum of ≈ 0.8 at high redshifts ($z \gtrsim 1$). In the EMSS band, the minimum K-correction would be ≈ 0.9 . These changes to the K-corrections are small compared to the luminosity evolution observed (e.g. for $L \propto (1+z)^3$, a change in luminosity by a factor of nine from $z=0.4$ to $z=2$). Thus we would expect the detailed values of the XLF parameters to change slightly, but not the general conclusions, including which evolutionary models produce acceptable fits to the data.

4.6 Narrow Emission Line Galaxies

Sixteen of the ROSAT X-ray sources have been identified with narrow emission line galaxies (NELGs) by M^cHardy *et al.* (1996). From optical emission line diagnostics, some may contain absorbed AGN. Since the EMSS also contains examples of this class of source, and these are included in the EMSS AGN sample we have used here, we have investigated the effect of including the ROSAT NELGs in the analysis. All the NELGs, in both ROSAT and EMSS samples, lie

at redshifts $z < 0.6$, so their inclusion is unlikely to affect the high redshift XLF behaviour. The luminosities of the ROSAT NELGs lie in the range 3×10^{41} - 10^{43} erg s $^{-1}$, but we have only included NELGs of luminosity $> 10^{42}$ erg s $^{-1}$ in the analysis, in order to maintain consistency with the previous analysis which used a lower limit of 10^{42} erg s $^{-1}$ in the maximum likelihood calculation, and because galaxies below this luminosity are more likely to be normal or star-forming galaxies, not containing AGN. Above this luminosity, there were 12(13) NELGs for $q_0=0.5(0)$.

The results are given in Table 2, models E to H. In general, the only effect is to increase the low luminosity slope of the XLF by ≈ 0.15 (not surprising given the low luminosities of the NELGs). All other parameters are virtually unchanged. A redshift cutoff in the luminosity evolution at $z_{cut} \approx 1.4$ is still required for $q_0=0.5$.

The nature of the NELGs, and the origin of their X-ray emission, is not well understood at present. The redshift distributions of the NELGs and the QSOs are clearly very different; the NELG+QSO $n(z)$ is plotted as a dashed line in Figure 2. We argue here that the NELG population cannot consist completely of low luminosity AGN because of the double-peaked shape of this $n(z)$ distribution. Although the evolutionary models with a relatively steep low luminosity XLF slope produce acceptable fits to the ROSAT and EMSS data combined, they do not produce a double peaked redshift distribution, as shown by the $n(z)$ prediction of model H in Figure 2. A one-dimensional KS test on the unbinned data finds the $n(z)$ distribution of the combined ROSAT QSOs and NELGs only marginally consistent with the prediction of model H at the 4% level, whereas the $n(z)$ distribution of the ROSAT QSOs alone is consistent with the prediction of model D at the $>20\%$ level. In order to produce a double peaked QSO redshift distribution, a re-steepening of the low luminosity XLF slope would be required at the lowest luminosities, beyond the ‘flat’ portion of the XLF ($L \lesssim 10^{43}$ erg s $^{-1}$ and $z \sim 0.3$). No such re-steepening was observed by Maccacaro *et al.* (1991) in their $0 < z < 0.18$ EMSS XLF which extended to luminosities of 10^{42} erg s $^{-1}$, and included the EMSS NELGs. The NELGs may have highly absorbed X-ray spectral components which are undetected in soft X-ray surveys. However, no evidence for a large column density ($> 10^{21}$ cm $^{-2}$) in the ROSAT NELG spectra was found by Romero Colmenero *et al.* (1996) and the relatively faint optical fluxes of the NELGs do not imply very large X-ray fluxes (M^cHardy *et al.* 1996). A simpler explanation is that some fraction of the NELGs, or some fraction of their X-ray emission, is from a different, non AGN, origin.

5 THE QSO CONTRIBUTION TO THE SOFT X-RAY BACKGROUND

In order to estimate the total QSO contribution to the 1-2 keV X-ray background (XRB), including the contribution from QSOs of flux fainter than the limit of the ROSAT survey, we integrated the evolving QSO XLF, including luminosities and redshifts which have not been directly sampled by any survey. The intensity of the 1-2 keV extragalactic XRB was taken to be 1.25×10^{-8} erg cm $^{-2}$ s $^{-1}$ sr $^{-1}$, as measured by Hasinger *et al.* (1993) and confirmed by Genetreau *et al.* (1995). The integration was performed over the

Table 3. QSO contribution to the 1-2 keV XRB.

| Model | q_0 | I_Q , 10^{-8} erg cm $^{-2}$ s $^{-1}$ sr $^{-1}$ (0.3-3.5 keV) | XRB fraction (per cent) |
|-------|-------|--|----------------------------|
| B | 0.5 | 1.37 | 31% |
| C | 0.0 | 2.23 | 50% |
| D | 0.0 | 2.05 | 46% |
| F | 0.5 | 1.58 | 35% |
| H | 0.0 | 2.28 | 51% |

redshift range $0 < z < 4$ and over the fixed luminosity range $10^{42} < L < 10^{48}$ erg s $^{-1}$. Since the XLF was measured in the 0.3-3.5 keV band, the values of the integrated QSO surface brightness, I_Q , were multiplied by 0.28 to convert to the 1-2 keV band, assuming an X-ray spectral index of 1. The values of I_Q and the corresponding XRB fractions are given in table 3 for various models which give good evolutionary fits. The 1-2 keV XRB fractions range from 31% to 51%.

The XRB fraction depends most strongly on the assumed cosmology; the values for $q_0=0$ are $\approx 50\%$ and those for $q_0=0.5$ are $\approx 35\%$. Smaller differences are caused by assuming that all of the X-ray luminosity of the ROSAT NELGs arise in AGN, and including them in the analysis (models F and H), or by the existence or not of a halt in the XLF luminosity evolution (models C and D).

The lower luminosity limit of 10^{42} erg s $^{-1}$ was chosen because this is the lower limit of the observed XLF at redshift zero. The surface density of QSOs contributing to the XRB using this lower limit varies from 2000 deg $^{-2}$ to 30000 deg $^{-2}$ depending on the model. Decreasing the lower luminosity limit to 10^{40} erg s $^{-1}$ increases the XRB contributions of most of the models by 2-4%, up to a maximum of 9% for model H, and increases the assumed QSO surface density to 2×10^4 deg $^{-2}$ to $\sim 10^6$ deg $^{-2}$, of the same order as the total surface density of all the faintest galaxies currently observed. At these low luminosities, the AGN luminosity would in any case be similar to the host galaxy X-ray luminosity. The sensitivity of model H, which includes the ROSAT NELGs, to the lower luminosity limit is because model H has the steepest value of the low luminosity XLF slope ($\alpha_1=1.78$) of any of the models considered here. Apart from the assumed cosmology, the uncertainty in the low luminosity XLF slope (α_1) contributes the largest uncertainty of any of the XLF or evolutionary parameters. The uncertainty in the XRB contribution corresponding to the 68% confidence range in α_1 for model B, leaving the other parameters unchanged, is 31% (+9%,-7%) for a lower luminosity limit of 10^{42} erg s $^{-1}$, and 31% (+15%,-7%) for a lower limit of 10^{40} erg s $^{-1}$.

A recent measurement of the absolute 1-2 keV extragalactic XRB intensity incorporating ASCA and ROSAT data gives a value of 1.46×10^{-8} erg cm $^{-2}$ s $^{-1}$ sr $^{-1}$ (Chen, Fabian & Gendreau 1996). Using this higher value would decrease the measured QSO contributions from 31%-51% to 27%-44%.

6 CONCLUSIONS

We have performed a very deep ROSAT X-ray survey and measured the highest yet QSO surface density of 230 ± 40 deg $^{-2}$. A break in the QSO log(N)-log(S) relation has been

found at a flux of $\approx 2 \times 10^{-14}$ erg cm $^{-2}$ s $^{-1}$ (0.3-3.5 keV). We have shown that measurement of the QSO XLF at luminosities fainter than the break in the XLF at $z > 2.2$ is possible with very deep ROSAT surveys.

From a combination of the *Einstein* EMSS and our deep ROSAT survey, we find that pure luminosity evolution of the form $L_X \propto (1+z)^{3.0(+0.2,-0.3)}$ is a good description of the QSO XLF evolution at low redshifts. This evolution is consistent with that found in previous X-ray surveys, including from the EMSS alone, when the same evolutionary model is used in the comparison.

At higher redshifts, we find that a halt, or strong slowing, of the luminosity evolution is required at a redshift of $z=1.4$ (+0.4,-0.17) (for $q_0=0.5$). For $q_0=0$, the combined surveys are consistent with a halt to the evolution at $z=1.6$ (+0.37,-0.27), but the data do not require the halt. These conclusions are still valid if all the narrow emission line galaxies found in the ROSAT survey are assumed to be absorbed AGN. In fact, the very different redshift distributions of the QSOs and the narrow emission line galaxies suggest that some fraction of the X-ray flux from the narrow emission line galaxies arises from a non-AGN source.

Unexplained differences in the evolution parameters derived from optically selected surveys (e.g. $k=3.45$, $z_{cut}=1.9$, Boyle *et al.* 1991) and X-ray selected surveys exist. The change in slope with redshift of the high luminosity part of the optical LF observed in recent optical surveys is also not observed in X-ray surveys. Accurate treatment of the errors on the evolutionary parameters and future X-ray samples (both shallow and deep) will help resolve the differences.

We find that QSOs contribute between 31% and 51% of the 1-2 keV extragalactic X-ray background. Finally, we note that the errors on the parameters describing the luminosity function and its evolution may have been underestimated in some previous surveys.

7 ACKNOWLEDGEMENTS

We thank Mike Irwin for obtaining APM measurements, and acknowledge discussion of AGN X-ray spectra with Paul Nandra. We also thank the following observatories and their staff for support of this project: the Canada-France-Hawaii Telescope, the UK William Herschel Telescope, the Nordic Optical Telescope, the University of Hawaii 88 inch Telescope the Michigan-Dartmouth-MIT Telescope and the Very Large Array Radio Telescope. This work was supported by grants to a number of authors from the UK Science and Engineering Research Council and Particle Physics and Astronomy Research Council. KOM acknowledges support from the Royal Society. Summer student Scott Moore performed some of the CCD data reduction.

REFERENCES

- Avni, Y., & Bahcall, J.N., 1980, ApJ, 325, 694.
- Barcons, X., Branduardi-Raymont, G., Warwick, R.S., Fabian, A.C., Mason, K.O., M^cHardy, I.M., Rowan-Robinson, M., 1994, MNRAS, 268, 833.
- Boyle, B.J., Shanks, T., Perterson, B., 1988, MNRAS, 238, 957.
- Boyle, B.J., Jones, L.R., Shanks, T., Marano, B., Zitelli, V.,

- Zamorani, G., 1991, in "The Space Distribution of Quasars", ASP Conference Series Vol 21, ed Crampton, D.
- Boyle, B.J., Griffiths, R.E., Shanks, T., Stewart, G.C., Georgantopoulos, I., 1993, MNRAS, 260, 49.
- Boyle, B.J., Shanks, T., Georgantopoulos, I., Stewart, G.C. Griffiths, R.E., 1994, MNRAS 271, 639.
- Boyle, B.J., McMahon, R.G., Wilkes, B.J., Elvis, M., 1995, MNRAS, 272, 462.
- Branduardi-Raymont, G. *et al.* 1994, MNRAS, 270, 947.
- Briel, U.G. *et al.* 1995, "The ROSAT Users Handbook", MPE.
- Cash, W., 1979, ApJ 228, 939.
- Chen, L.-W., Fabian, A.C., Gendreau, K.C., MNRAS, in press.
- Ciliegi, P., Elvis, M., Wilkes, B.J., Boyle, B.J., McMahon, R.G., Maccacaro, T., 1995, MNRAS, 277, 1463.
- Della Ceca, R., Maccacaro, T., Gioia, I.M., Wolter, A., Stocke, T.J., 1992, ApJ, 389, 491.
- Fabian, A.C., *et al.* 1994, PASJ, 46, L59.
- Fasano, G., Franceschini, A. 1987, MNRAS, 225, 155.
- Franceschini, A., La Franca, F., Cristiani, S., Martin-Mirones, J.M., 1994, MNRAS, 269, 683.
- Fruscione, A., Griffiths, R.E., 1991, ApJ 380, L13.
- Gendreau, K.C., *et al.* 1995. PASJ, 47, 5.
- Halpern, J.P., Helfand, D.J., Moran, E.C., 1995, ApJ, 453, 611.
- Hasinger, G., Burg, R., Giacconi, R., Hartner, G., Schmidt, M., Trumper, J., Zamorani, G., 1993, A&A 275, 1.
- Hasinger, G., Boese, G., Predehl, P., Turner, T.J., Yusaf, R., George, I. & Rohrbach, G., 1993b, MPE/OGIP Calibration Memo Cal/Ros/93-015.
- Hewett, P.C., Foltz, C.B., Chaffee, F.H. 1993, ApJ, 406, L43.
- Jones, L.R., *et al.* 1994, Proc. of 35th Herstmonceux Conference, eds Maddox, S. and Aragon-Salamanca, A., World Scientific Publishing, p.339.
- Lampton, M. Margon, B., Bowyer, S. 1976, ApJ 208, 177.
- M^cHardy, I.M., *et al.* 1996, MNRAS submitted.
- Maccacaro, T., Della Ceca, R., Gioia, I.M., Morris, S.L., Stocke, J.T., Wolter, A., 1991, ApJ, 374, 117.
- Marshall, H.L., Avni, Y., Tananbaum, H., Zamorani, G., 1983, ApJ, 269, 35.
- Metcalfe, N., Shanks, T., Fong, R., Jones, L.R., 1991, MNRAS, 249, 498.
- Miller, L., Goldschmidt, P., La Franca, F., Cristiani, S., 1993, in Observational Cosmology, ASP Conf. Ser. vol 51, eds, G. Chincarini, *et al.*
- Nandra, P., Pounds, K.A., 1994, MNRAS, 268, 405.
- Otani, C. *et al.* 1996a, PASJ, in press.
- Otani, C. *et al.* 1996b, Proc. "Roentgenstrahlung from the Universe", in press.
- Page, M.J., Carrera, F.J., Hasinger, G., Mason, K.O., McMahon, R., Mittaz, J.P.D., Barcons, X., Carballo, R., Gonzalez-Serrano, I., Perez-Fournon, I., 1996, MNRAS, in press.
- Press, W.H., Teukolsky, S.A., Vetterling, W.T. & Flannery, B.P. 1992, Numerical Recipes, 2nd edition, Cambridge University Press.
- Romero Colmenero, E., Branduardi-Raymont, G., Carrera, F.J., Jones, L.R., Mason, K.O., McHardy, I.M., Mittaz, J.P.D., 1996, MNRAS, in press.
- Shanks, T., Georgantopoulos, I., Stewart, G.C., Pounds, K.A., Boyle, B.J. and Griffiths, R.E. 1991. Nature, 353, 315.
- Stocke, J.T., Morris, S.L., Gioia, I.M., Maccacaro, T., Schild, R., Wolter, A., Fleming, T.A., Henry, J.P., 1991, ApJS, 76, 813.
- Wilkes, B.J., Elvis, M., 1987, ApJ, 323, 243.
- Williams, O.R. *et al.* 1992, ApJ, 389, 157.